Hindawi
Wireless Communications and Mobile Computing
Volume 2021, Article ID 6635220, 10 pages
https://doi.org/10.1155/2021/6635220

Research Article

Gridless Multiple Measurements Method for One-Bit DOA Estimation with a Nested Cross-Dipole Array

Haining Long, Ting Su, Xianpeng Wang, and Mengxing Huang

Information and Communication Engineering, Hainan University, Hai Kou 570228, China

Correspondence should be addressed to Ting Su; suting4190@hainanu.edu.cn and Xianpeng Wang; wxpeng1986@126.com

Received 25 November 2020; Revised 8 January 2021; Accepted 17 August 2021; Published 31 August 2021

Academic Editor: Daniele Pinchera

The gridless one-bit direction of arrival (DOA) estimator is proposed to estimate electromagnetic (EM) sources on a nested cross-dipole array, and the multiple measurement vectors (MMV) mode is introduced to improve the reliability of parameter estimation. The gridless method is based on atomic norm minimization, solved by alternating direction multiplier method (ADMM). With gridless method used, sign inconsistency caused by one-bit measurements and basis mismatches by traditional grid-based algorithms can be avoided. Furthermore, the reconstructed denoising measurements with fast convergence and stable recovery accuracy are obtained by ADMM. Finally, spatial smoothing root multiple signal classification (SSRMUSIC) and dual polynomial (DP) methods are used, respectively, to estimate the DOAs on the reconstructed denoising measurements. Numerical results show that our method one-bit ADMM-SSRMUSIC has a better performance than that of one-bit SSRMUSIC used directly. At low signal to noise ratio (SNR) and low snapshot, the one-bit ADMM-DP has an excellent performance which is even better than that of unquantized MUSIC. In addition, the proposed methods are also suitable for both completely polarized (CP) signals and partially polarized (PP) signals.

1. Introduction

Since electromagnetic (EM) source signal carries the complete information buried in the fields, the direction finding of the EM source signal has a wide application. For instance, the direction of arrival (DOA) estimation of EM source signals was solved, respectively, by rotational invariance technique (ESPRIT) algorithm [1–3], maximum likelihood (ML) algorithm [4], and multiple signal classification- (MUSIC-) based solution [5]. The performance of parameter estimation is closely related to the array structures [6]. For a uniform linear array (ULA), N sensors can only restore $N-1$ sources at most [7, 8]. As a result, a large-scale ULA is needed for estimating multiple source signals, and the power consumption of analog-to-digital converters (ADC) increases exponentially.

A sparse array is a viable alternative, which can generate virtual sensors by using the position relation among physical sensors and obtain more degree of freedoms (DOFs). Sparse arrays mainly include minimum redundancy arrays (MRA) [9], nested arrays [10], coprime arrays [11], and other sparse arrays based on them [12, 13]. The reversed and shift sparse array based on the difference and sum coarray is proposed for longer consecutive virtual array [14]. A novel sparse array with displaced multistage cascade subarrays is proposed to obtain high DOF [15]. [16] increases the DOF by using synthetic aperture technology and the concept of difference coarray. Moreover, the nested array is widely concerned for its unique and continuous virtual array elements and simple construction [17]. In [18], a nested cross-dipole array is used to estimate the DOA of EM source signals with spatial smoothing MUSIC (SS-MUSIC). Nevertheless, the hardware cost of ADC is still at a high level for large-scale nested cross-dipole arrays. One-bit measurements are popular to decline the consumption [19–21]. In [22], one-bit SS-MUSIC is proposed for DOA estimation of EM source signals.

In [23], the authors present that sign inconsistency are induced by one-bit measurements with additive noises and an atomic norm minimization with a linear loss function can overcome the shortage. Meanwhile, as a gridless method, atomic norm minimization can avoid the basis mismatches caused by discretization of the signal parameter space [24, 25]. The alternating direction multiplier method (ADMM) is proposed to solve the atomic norm minimization with one-bit quantization in the single measurement vector (SMV) model [23, 26, 27]. ADMM has lower computational complexity and higher convergence speed compared with the semidefinite programming (SDP) [28].

In this paper, the atomic norm minimization with ADMM is extended for reconstructing the one-bit EM source signals using a nested cross-dipole array. The multiple measurement vectors (MMV) model is used instead of the SMV model. The MMV model has a higher success rate to reconstruct unknown signals compared with that of the SMV model. And then, two DOA estimation methods based on the constructed denoising measurements are proposed, spatial smoothing root-MUSIC (SSRMUSIC) algorithm [22] and dual polynomial (DP) method [23, 29]. In order to highlight the advantage of ADMM in signal reconstruction, SSRMUSIC algorithm with constructed denoising measurements will be compared with ordinary one-bit SSRMUSIC algorithm. And SSRMUSIC is robust in high SNR and multiple snapshots, but with the decrease of SNR and snapshot number, its resolution decreases rapidly. Therefore, the DP method is introduced for high recovery accuracy in low SNR and low snapshot. The main contributions of this paper are as follows: (1) The formulas of one-bit ADMM are derived to estimate DOAs of EM source signals using a nested cross-dipole array, and the MMV model is used instead of SMV to improve estimation accuracy. (2) With the gridless method based on atomic norm used, the sign inconsistency caused by one-bit quantization and basis mismatches by grid discretization are both avoid. (3) Two methods, SSRMUSIC and DP method, are used to solve the proposed problem, respectively. Simulation results show that one-bit ADMM SSRMUSIC has a better performance than that of one-bit SSRMUSIC used directly, while one-bit ADMM DP has an excellent performance in the situation of low signal to noise ratio (SNR) and low snapshot. (4) Most of the algorithms [30–32] for estimating the space parameters of both completely polarized (CP) signals and partially polarized (PP) signals are not universal. Our proposed algorithms are suitable for both CP signals and PP signals.

The rest of this paper is structured as follows. Section 2 describes the signal model of a nested cross-dipole array. The one-bit quantization model and difference coarray are introduced in Section 3. Section 4 presents the atomic norm minimization for the MMV model. The one-bit ADMM formulas and two methods for DOA estimation are also derived in Section 4. Simulation results are given and analysed to verify the efficiency and accuracy of the proposed algorithms in Section 5. Section 6 summarizes this paper.

Notations are as follows: $\Re\{\mathbf{X}\}$ and $\Im\{\mathbf{X}\}$ are real part and imaginary part of $\mathbf{X}$, respectively. $\mathbf{I}_M$ is the identity matrix by $M \times M$ and $\mathbf{T}(\mathbf{u})$ denotes the Toeplitz matrix whose first column is $\mathbf{u}$.Tr$(\mathbf{X})$, det $(\mathbf{X})$, $\langle \mathbf{X} \rangle_R$, vec$(\mathbf{X})$, and $E(\mathbf{X})$ present the trace, the determinant, the real inner product, the vectorization, and the expectation of $\mathbf{X}$, respectively. $\mathbf{X}^\dagger$, $\mathbf{X}^H$, $\mathbf{X}^T$, and $\mathbf{X}^*$ denote the Moore-Penrose pseudoinverse, the conjugate transpose matrix, the transpose, and the conjugation of $\mathbf{X}$, respectively. $\boldsymbol{conj}(\cdot)$ means the conjugate operation on each entry of a vector or a matrix. $\mathbf{e}_1$ is a vector where the first element is 1, and the rest are 0. inf $(\cdot)$ means the infimum operator. conv$(\mathscr{A})$ is the convex hull of $\mathscr{A}$. $\|\cdot\|_{\mathscr{A}}^*$ is the dual atomic norm.

2. Signal Model

Suppose that K narrowband EM source signals impinge onto a nested cross-dipole array, the sensors with locations $\{d_1 d, d_2 d, \cdots, d_M d\}$, $d_m \in \mathbb{S}$, $m = 1, \cdots, M$. M is the number of elements, $M = M_1 + M_2$. The unit interelement spacing d is usually set as half-wavelength. The signal model is shown in Figure 1. Each cross-dipole consists of two dipoles parallel to the x-axis and y-axis, respectively [18]. Consequently, the received signals for x-axis and y-axis at sensor m can be given by

$$x_m^{[l]}(t) = \sum_{k=1}^{K} B_k^{[l]} s_k^{[l]}(t) a_m\left(\bar{\theta}_k\right) + n_m^{[l]}(t) \; l = x, y, \tag{1}$$

where θ_k and $\bar{\theta}_k$ denote the DOA and the normalized DOA of the $\boldsymbol{k}\boldsymbol{th}$ source, respectively. $\theta_k \in [-\pi/2, \pi/2]$, $\bar{\theta}_k = \sin \theta_k/2$, and $\bar{\theta}_k \in [-1/2, 1/2]$. $a_m(\bar{\theta}_k) = e^{j2\pi\bar{\theta}_k d_m}$ is the spatial response of the $\boldsymbol{m}\boldsymbol{th}$ dipole for the $\boldsymbol{k}\boldsymbol{th}$ source. $B_k^{[l]}$and $s_k^{[l]}(t)$ present the cross-dipole response and signal for l-axis of the $\boldsymbol{k}\boldsymbol{th}$ source. Moreover, $B_k^{[x]} = -1$ and $B_k^{[y]} = \cos\,(\arcsin 2\bar{\theta}_k)$. $n_m^{[l]}(t)$ is the noise component for l-axis at the $\boldsymbol{m}\boldsymbol{th}$ sensor. When x-axis and y-axis are considered simultaneously, $x_m^{[l]}(t)$, $n_m^{[l]}(t)$, and $s_k^{[l]}(t)$ can be written as vectors: $\mathbf{x}_m(t) = [x_m^{[x]}(t), x_m^{[y]}(t)]^T$, $\mathbf{n}_m(t) = [n_m^{[x]}(t), n_m^{[y]}(t)]^T$, and $\mathbf{s}_k(t) = [s_k^{[x]}(t), s_k^{[y]}(t)]^T$. The covariance of $\mathbf{s}_k(t)$ is given by [4].

$$\mathbf{R}_{\mathbf{s}_k} = E\left[\mathbf{s}_k(t)\mathbf{s}_k^H(t)\right] = \frac{p_{k_{UP}}^2}{2}\mathbf{I}_2 + p_{k_{CP}}^2 \boldsymbol{\Phi}(\alpha_k)\mathbf{w}(\beta_k)\mathbf{w}^H(\beta_k)\boldsymbol{\Phi}^H(\alpha_k), \tag{2}$$

where

$$\boldsymbol{\Phi}(\alpha_k) = \begin{bmatrix} \cos\,(\alpha_k) & \sin\,(\alpha_k) \\ -\sin\,(\alpha_k) & \cos\,(\alpha_k) \end{bmatrix}, \tag{3}$$

$$\mathbf{w}(\beta_k) = [\cos\,(\beta_k)\; j \sin\,(\beta_k)]^T, \tag{4}$$

with $\alpha_k \in (-\pi/2, \pi/2)$ and $\beta_k \in (-\pi/4, \pi/4)$ being the polarization orientation angle and polarization ellipticity angle, respectively. $p_{k_{CP}}^2$ and $p_{k_{UP}}^2$ denote the power of the kth source

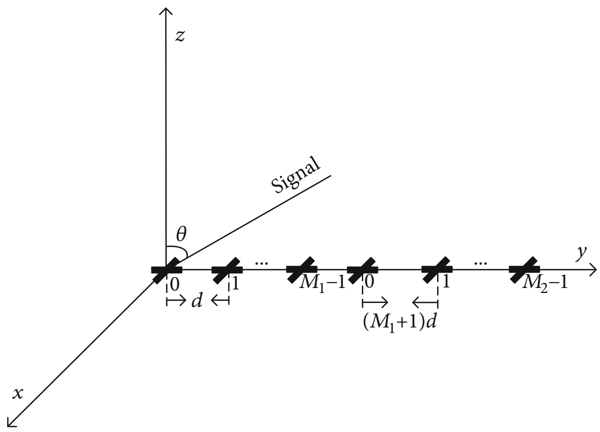

Figure 1: Nested array of cross-dipoles [22].

of CP signals and unpolarized (UP) signals, respectively. The degree of polarization (DOP) of $\mathbf{s}_k(t)$ can be calculated from the $\mathbf{R}_{s_k}$.

$$\eta_k = \left[1 - \frac{4\det\left(\mathbf{R}_{s_k}\right)}{\left[\mathrm{Tr}\left(\mathbf{R}_{s_k}\right)\right]^2}\right]^{1/2}. \tag{5}$$

Moreover, η_k is defined as the ratio of CP component power to total signal power [4].

$$\eta_k = \frac{p_{k_{CP}}^2}{p_{k_{CP}}^2 + p_{k_{UP}}^2}. \tag{6}$$

The DOPs of CP signals and UP signals are $\eta_k = 1$ and $\eta_k = 0$, respectively, and that of PP signals is $\eta_k \in (0, 1)$. CP signal of the kth source is expressed as

$$\mathbf{s}_k(t) = \begin{bmatrix} \cos\varphi_k \\ e^{j\psi_k}\sin\varphi_k \end{bmatrix} \tilde{s}_k(t), \tag{7}$$

where $\varphi_k \in [0, \pi/2]$ and $\psi_k \in (-\pi, \pi]$ are polarization parameters, representing auxiliary polarization angle and the auxiliary polarization phase difference, respectively [20]. The covariance matrix $\mathbf{R}_{s_k}$ of CP signals and UP signals are all rank 2. Since PP signals can be expressed as the superposition of CP signals and UP signals, PP signals of the kth source can be expressed as

$$\mathbf{s}_k(t) = \left\{ \sqrt{\eta_k}\begin{bmatrix} \cos\varphi_k \\ e^{j\psi_k}\sin\varphi_k \end{bmatrix} + \sqrt{\frac{1-\eta_k}{2}}\begin{bmatrix} \beta_1(t) \\ \beta_2(t) \end{bmatrix} \right\} \tilde{s}_k(t). \tag{8}$$

Both $\beta_1(t)$ and $\beta_2(t)$ are Gaussian random processes with zero mean. The covariance matrix $\mathbf{R}_{s_k}$ of PP signals is rank deficient.

Consider the dipoles measurements of x-axis and y-axis, Equation (1) can be written as

$$\mathbf{x}_{\mathbb{S}}^{[l]}(t) = \sum_{k=1}^{K} B_k^{[l]} s_k^{[l]}(t)\mathbf{a}_{\mathbb{S}}\left(\overline{\theta}_k\right) + \mathbf{n}_{\mathbb{S}}^{[l]}(t) \quad l = x, y, \tag{9}$$

where $\mathbf{x}_{\mathbb{S}}^{[l]}(t) = [x_1^{[l]}(t), \cdots, x_M^{[l]}(t)]$ is the array response of l-axis, $\mathbf{a}_{\mathbb{S}}(\overline{\theta}_k) = [a_1(\overline{\theta}_k), \cdots, a_M(\overline{\theta}_k)]^T$ is the steering vector, and $\mathbf{n}_{\mathbb{S}}^{[l]}(t) = [n_1^{[l]}(t), \cdots, n_M^{[l]}(t)]^T$ denotes the additive noise of l-axis. Moreover, the source signals $\{s_1^{[l]}(t), \cdots, s_K^{[l]}(t)\}$ are assumed to be independent random Gaussian processes. The additive noise $\mathbf{n}_{\mathbb{S}}^{[l]}(t)$ is an independent additive complex white Gaussian process with distribution $\mathscr{CN}(0, (\sigma^{[l]})^2\mathbf{I}_M)$. The covariance of $\mathbf{x}_{\mathbb{S}}^{[l]}(t)$ is

$$\begin{aligned} \mathbf{R}_{\mathbf{x}_{\mathbb{S}}^{[l]}} &= E\left[\mathbf{x}_{\mathbb{S}}^{[l]}(t)\left(\mathbf{x}_{\mathbb{S}}^{[l]}(t)\right)^H\right] \\ &= \sum_{k=1}^{K}\left(p_k^{[l]}\right)^2 \mathbf{a}_{\mathbb{S}}^{[l]}\left(\overline{\theta}_k\right)\left(\mathbf{a}_{\mathbb{S}}^{[l]}\left(\overline{\theta}_k\right)\right)^H + \left(\sigma^{[l]}\right)^2\mathbf{I}_M, \end{aligned} \tag{10}$$

where $(p_k^{[l]})^2$ and $(\sigma^{[l]})^2$ denote the source power and noise power of the kth source of l-axis, respectively.

3. One-Bit Quantization

The one-bit quantizer can be implemented by a sign operation, which is defined as

$$\boldsymbol{sign}(x) = \begin{cases} -1, x \le 0, \\ 1, x > 0. \end{cases} \tag{11}$$

After one-bit quantizer, only the symbol information is left. Although the one-bit quantizer does not reduce the computational complexity, it greatly reduces the hardware consumption compared with the unquantized algorithm. Equation (9) is modified as

$$\mathbf{y}_{\mathbb{S}}^{[l]}(t) = \frac{1}{\sqrt{2}}\left[\mathrm{sign}\left(\Re\left\{\mathbf{x}_{\mathbb{S}}^{[l]}(t)\right\}\right) + j\,\mathrm{sign}\left(\Im\left\{\mathbf{x}_{\mathbb{S}}^{[l]}(t)\right\}\right)\right]. \tag{12}$$

The factor $1/\sqrt{2}$ normalizes the power of $\mathbf{y}_{\mathbb{S}}^{[l]}(t)$ [19]. $\mathbf{y}_{\mathbb{S}}^{[x]}$ and $\mathbf{y}_{\mathbb{S}}^{[y]}$ are rewritten as $\mathbf{Y}_{\mathbb{S}}^{[x]}$ and $\mathbf{Y}_{\mathbb{S}}^{[y]}$ in multiple snapshots. The covariance matrices corresponding to $\mathbf{Y}_{\mathbb{S}}^{[x]}$ and $\mathbf{Y}_{\mathbb{S}}^{[y]}$ are approximated by the sample covariance, expressed as $\widehat{\mathbf{R}}_{\mathbf{Y}_{\mathbb{S}}^{[x]}}$ and $\widehat{\mathbf{R}}_{\mathbf{Y}_{\mathbb{S}}^{[y]}}$, respectively.

$$\widehat{\mathbf{R}}_{\mathbf{Y}_{\mathbb{S}}^{[l]}} = \frac{1}{N}\sum_{n=1}^{N}\mathbf{Y}_{\mathbb{S}}^{[l]}(n)\left(\mathbf{Y}_{\mathbb{S}}^{[l]}(n)\right)^H. \tag{13}$$

We combine the DOA estimation with the difference coarray instead of the original array. The number of estimable sources is closely related to the structure of the array. The difference coarray corresponding to $\mathbb{S}$ is defined as $\mathbb{D} = \{d_i - d_j | \forall d_i, d_j \in \mathbb{S}\}$. Specifically, the difference coarray of the nested array can be expressed as$\mathbb{D} = \{1 - M_2(M_1 + 1), \cdots, 0, \cdots, M_2(M_1 + 1) - 1\}$. $D_{\max} = M_2(M_1 + 1) - 1$, where $D_{\max}$ is the maximum number of DOFs [10]. The difference coarray thus occurs naturally in problems involving second-order statistics of the received signals [10]. The one-bit autocorrelation vectors of the difference coarray $\mathbb{D}$ for the x-axis and y-axis are defined as follows:

$$\mathbf{y}_{\mathbb{D}}^{[l]} = \mathbf{J}^{\dagger} \mathrm{vec}\left(\widehat{\mathbf{R}}_{\mathbf{Y}_{\mathbb{S}}^{[l]}}\right). \tag{14}$$

The definition of binary matrix $\mathbf{J}$ is the same as [33], with size $|\mathbb{S}|^2 - \boldsymbol{by} - |\mathbb{D}|$. The columns of $\mathbf{J}$ satisfy $\langle \mathbf{J} \rangle_{:,\tilde{d}} = [\mathrm{vec}(\tilde{\mathbf{J}}(\tilde{d}))]^T, \tilde{d} \in \mathbb{D}$, where $\tilde{\mathbf{J}}(\tilde{d}) \in \{0, 1\}^{|\mathbb{S}| \times |\mathbb{S}|}$ is given by

$$\left\langle \tilde{\mathbf{J}}\left(\tilde{d}\right) \right\rangle_{d_i, d_j} = \begin{cases} 1, & \text{if } d_i - d_j = \tilde{d}, \\ 0, & \text{otherwise.} \end{cases} \forall d_i, d_j \in \mathbb{S} \tag{15}$$

4. The Proposed Methods

4.1. One-Bit Multiple Snapshots Model with Atomic Norm Minimization. The atomic norm is used to find the minimum number of atoms in the continuous parameter space; then, the basis mismatches by grid discretization will be avoided. And the linear loss function with characteristics of one-bit quantization will overcome the sign inconsistency caused by one-bit quantization. In order to make use of the joint sparsity between $\mathbf{y}_{\mathbb{D}}^{[x]}$ and $\mathbf{y}_{\mathbb{D}}^{[y]}$, the following definition is given:

$$\mathbf{Y} = \left[\mathbf{y}_{\mathbb{D}}^{[x]}, \mathbf{y}_{\mathbb{D}}^{[y]}\right]. \tag{16}$$

In Equation (16), $\mathbf{Y}$ is defined as the multiple snapshots (two snapshots) measurements. Let $\mathbf{X}$ be the denoising signal of $\mathbf{Y}$ and defines an atom to represent $\mathbf{X}$ as

$$\mathbf{A}(f, \mathbf{b}) = \mathbf{a}_{\mathbb{D}}(f)\mathbf{b}^H \in \mathscr{A}, \tag{17}$$

where $f \in [0, 1), \mathbf{b} \in \mathbb{C}^L$, $\|\mathbf{b}\|_2 = 1$, and $\mathscr{A}$ is the set of atoms. We assume that no element $\mathbf{A} \in \mathscr{A}$ lies in the convex hull of the other elements $\mathrm{conv}(\mathbf{A} \setminus \mathscr{A})$, i.e., the elements of $\mathscr{A}$ are the extreme points of $\mathrm{conv}(\mathscr{A})$ [34]. $\mathscr{A}$ is defined as

$$\mathscr{A} = \left\{\mathbf{A}(f, \mathbf{b}) \mid f \in [0, 1), \|\mathbf{b}\|_2 = 1\right\}, \tag{18}$$

where $\mathscr{A}$ is regarded as an infinite dictionary to describe the continuous changing parameters, and the atom of $\mathscr{A}$ is the basic unit to construct $\mathbf{X}$. $\|\mathbf{X}\|_{\mathscr{A},0}$ is defined to represent the minimum number of atoms describing $\mathbf{X}$ [29].

$$\|\mathbf{X}\|_{\mathscr{A},0} = \inf_K \left\{ \mathbf{X} = \sum_{k=1}^{K} c_k \mathbf{A}(f_k, \mathbf{b}_k), c_k \geq 0 \right\}. \tag{19}$$

Since the minimization of Equation (19) is a NP problem, we consider the convex relaxation of $\|\mathbf{X}\|_{\mathscr{A},0}$, denoted by $\|\mathbf{X}\|_{\mathscr{A}}$. $\|\mathbf{X}\|_{\mathscr{A}}$ denotes the gauge of $\mathscr{A}$, and the gauge function can be defined as [35, 36].

$$\begin{aligned} \|\mathbf{X}\|_{\mathscr{A}} &= \inf \{t > 0 : \mathbf{X} \in t\,\mathrm{conv}(\mathscr{A})\} \\ &= \inf \left\{ \sum_k c_k \middle| \mathbf{X} = \sum_k c_k \mathbf{A}(f_k, \mathbf{b}_k), c_k \geq 0 \right\}, \end{aligned} \tag{20}$$

where $\|\mathbf{X}\|_{\mathscr{A}}$ is called the atomic norm of $\mathbf{X}$, which actually adds a sparse constraint to $\mathscr{A}$ but without discretization.

Considering the characteristics of one-bit quantization, and to ensure consistent recovery and constrain the signals to the unit ball, a linear loss function is proposed to recover the signals.

$$\begin{aligned} \underset{\mathbf{X}_R, \mathbf{X}_S}{\arg\min} \quad & -\frac{1}{2|\mathbb{D}|}\left(\left(\mathbf{Y}_R^{\breve{l}}\right)^T \mathbf{X}_R^{\breve{l}} + \left(\mathbf{Y}_S^{\breve{l}}\right)^T \mathbf{X}_S^{\breve{l}}\right) + \tau\|\mathbf{X}\|_{\mathscr{A}}, \\ \boldsymbol{s.t.} \quad & \left\|\mathbf{X}_R^{\breve{l}}\right\|_1 + \left\|\mathbf{X}_S^{\breve{l}}\right\|_1 \leq 1, \end{aligned} \tag{21}$$

where $l \in L$, τ is regularization parameter, which is defined as

$$\tau = c\sqrt{L \log |\mathbb{D}|}, \tag{22}$$

where scale factor $c = 0.358$. It can be seen from Equation (16) that Equation (21) can be transformed into a matrix equation with dimension of 2×2 when $L = 2$. It is easy to know that only diagonal elements play an important role. Then, Equation (21) can be transformed into the formula about trace.

$$\begin{aligned} \underset{\mathbf{X}_R, \mathbf{X}_S}{\arg\min} \quad & -\frac{1}{2|\mathbb{D}|}\mathrm{Tr}\left(\mathbf{Y}_R^T\mathbf{X}_R + \mathbf{Y}_S^T\mathbf{X}_S\right) + \tau\|\mathbf{X}\|_{\mathscr{A}}, \\ \boldsymbol{s.t.} \quad & \mathrm{Tr}\left(\mathbf{Y}_R^T\mathbf{X}_R + \mathbf{Y}_S^T\mathbf{X}_S\right) \leq \mathrm{Tr}(\mathbf{I}_2). \end{aligned} \tag{23}$$

Equation (23) can be solved by the SDP problem.

$$\begin{aligned} \underset{\mathbf{X}_R, \mathbf{X}_S}{\arg\min} \quad & -\frac{1}{2\,|\,\mathbb{D}\,|}\mathrm{Tr}\left(\mathbf{Y}_R^T\mathbf{X}_R + \mathbf{Y}_S^T\mathbf{X}_S\right) + \frac{\tau}{2}[\mathrm{Tr}(\mathbf{T}(\mathbf{u})) + \mathrm{Tr}(\mathbf{W})], \\ \text{s.t.} \quad & \begin{bmatrix} \mathbf{T}(\mathbf{u}) & \mathbf{X}_R + j\mathbf{X}_S \\ (\mathbf{X}_R + j\mathbf{X}_S)^H & \mathbf{W} \end{bmatrix} \geq 0, \\ & \mathrm{Tr}\left(\mathbf{Y}_R^T\mathbf{X}_R + \mathbf{Y}_S^T\mathbf{X}_S\right) \leq \mathrm{Tr}(\mathbf{I}_2). \end{aligned} \tag{24}$$

The SDP problem can be solved by CVX [35]. However, the convergence speed of SDP is very slow.

4.2. ADMM for One-Bit Multiple Snapshot Model. In order to speed up the convergence speed and protect the accuracy of signal reconstructed, Equation (23) can also be solved by ADMM.

$$\begin{aligned}
&\underset{\mathbf{X}_R,\mathbf{X}_S}{\arg\min} \quad -\frac{1}{2|\mathbb{D}|}\mathrm{Tr}\left(\mathbf{Y}_R^T\mathbf{X}_R+\mathbf{Y}_S^T\mathbf{X}_S\right)+\frac{\tau}{2}[\mathrm{Tr}(\mathbf{T}(\mathbf{u}))+\mathrm{Tr}(\mathbf{W})],\\
&\boldsymbol{s.t.} \qquad \mathbf{Z}=\begin{bmatrix}\mathbf{T}(\mathbf{u}) & \mathbf{X}_R+j\mathbf{X}_S\\ (\mathbf{X}_R+j\mathbf{X}_S)^H & \mathbf{W}\end{bmatrix},\\
&\qquad\qquad \mathbf{Z}\geq 0,\\
&\qquad\qquad \mathrm{Tr}(\mathbf{G})=\mathrm{Tr}(\mathbf{I}_2)-\mathrm{Tr}\left(\mathbf{Y}_R^T\mathbf{X}_R\right)-\mathrm{Tr}\left(\mathbf{Y}_S^T\mathbf{X}_S\right),\\
&\qquad\qquad \mathrm{Tr}(\mathbf{G})\geq 0.
\end{aligned} \tag{25}$$

$\mathbf{Z}$, $\mathbf{\Lambda}$, and $\mathbf{W}$ are Hermitian matrices, $\mathrm{Tr}(\mathbf{G})$ is the dual variable, and the augmented Lagrangian corresponding to the above formula is

$$\begin{aligned}
&L(\mathbf{X}_R,\mathbf{X}_S,\mathbf{W},\mathbf{\Lambda},\mathbf{Z},\mathrm{Tr}(\mathbf{G}),\mathbf{u},\gamma)\\
&\quad=-\frac{1}{2|\mathbb{D}|}\mathrm{Tr}\left(\mathbf{Y}_R^T\mathbf{X}_R+\mathbf{Y}_S^T\mathbf{X}_S\right)\\
&\qquad+\frac{\tau}{2}[\mathrm{Tr}(\mathbf{T}(\mathbf{u}))+\mathrm{Tr}(\mathbf{W})]\\
&\quad=\left\langle \mathbf{\Lambda},\mathbf{Z}-\begin{bmatrix}\mathbf{T}(u) & \mathbf{X}_R+j\mathbf{X}_S\\ (\mathbf{X}_R+j\mathbf{X}_S)^H & \mathbf{W}\end{bmatrix}\right\rangle\\
&\quad=\frac{\rho}{2}\left\|\mathbf{Z}-\begin{bmatrix}\mathbf{T}(u) & \mathbf{X}_R+j\mathbf{X}_S\\ (\mathbf{X}_R+j\mathbf{X}_S)^H & \mathbf{W}\end{bmatrix}\right\|_F^2\\
&\quad=\gamma\mathrm{Tr}\left(\mathbf{G}-\mathbf{I}_2+\mathbf{Y}_R^T\mathbf{X}_R+\mathbf{Y}_S^T\mathbf{X}_S\right)\\
&\quad=\frac{\rho}{2}\left\|\mathbf{G}-\mathbf{I}_2+\mathbf{Y}_R^T\mathbf{X}_R+\mathbf{Y}_S^T\mathbf{X}_S\right\|_F^2,
\end{aligned} \tag{26}$$

where γ is the dual variable and ρ is the penalty parameter. Note that

$$\mathbf{Z}=\begin{bmatrix}\mathbf{Z}_0 & \mathbf{Z}_1\\ \mathbf{Z}_2 & \mathbf{Z}_3\end{bmatrix}=\begin{bmatrix}\mathbf{Z}_0 & \mathbf{Z}_{1_R}+j\mathbf{Z}_{1_S}\\ \left(\mathbf{Z}_{1_R}+j\mathbf{Z}_{1_S}\right)^H & \mathbf{Z}_3\end{bmatrix}, \tag{27}$$

$$\mathbf{\Lambda}=\begin{bmatrix}\mathbf{\Lambda}_0 & \mathbf{\Lambda}_1\\ \mathbf{\Lambda}_2 & \mathbf{\Lambda}_3\end{bmatrix}=\begin{bmatrix}\mathbf{\Lambda}_0 & \mathbf{\Lambda}_{1_R}+j\mathbf{\Lambda}_{1_S}\\ \left(\mathbf{\Lambda}_{1_R}+j\mathbf{\Lambda}_{1_S}\right)^H & \mathbf{\Lambda}_3\end{bmatrix}. \tag{28}$$

ADMM has the following update steps:

$$\left(\mathbf{X}_R^{t+1},\mathbf{X}_S^{t+1},\mathbf{W}^{t+1},\mathbf{u}^{t+1}\right)=\underset{\mathbf{X},\mathbf{W},\mathbf{u}}{\arg\min}\, L\left(\mathbf{X}_R,\mathbf{X}_S,\mathbf{W},\mathbf{u},\mathbf{\Lambda}^t,\mathbf{Z}^t,\mathrm{Tr}(\mathbf{G})^t,\gamma^t\right), \tag{29}$$

$$\left(\mathbf{Z}^{t+1},\mathrm{Tr}(\mathbf{G})^{t+1}\right)=\underset{\mathbf{Z},\mathrm{Tr}(\mathbf{G})}{\arg\min}\, L\left(\mathbf{X}_R^{t+1},\mathbf{X}_S^{t+1},\mathbf{W}^{t+1},\mathbf{u}^{t+1},\mathbf{\Lambda}^t,\mathbf{Z}^t,\mathrm{Tr}(\mathbf{G}),\gamma^t\right), \tag{30}$$

$$\mathbf{\Lambda}^{t+1}=\mathbf{\Lambda}^t+\rho\left(\mathbf{Z}^{t+1}-\begin{bmatrix}\mathbf{T}\left(\mathbf{u}^{t+1}\right) & \mathbf{X}_R^{t+1}+j\mathbf{X}_S^{t+1}\\ \left(\mathbf{X}_R^{t+1}+j\mathbf{X}_S^{t+1}\right)^H & \mathbf{W}^{t+1}\end{bmatrix}\right), \tag{31}$$

$$\gamma^{t+1}=\gamma^t+\rho\mathrm{Tr}\left(\mathbf{G}^{t+1}-\mathbf{I}_2+\mathbf{Y}_R^T\mathbf{X}_R^{t+1}+\mathbf{Y}_S^T\mathbf{X}_S^{t+1}\right). \tag{32}$$

The closed form expressions updated with the iteration times t can be obtained.

$$\mathbf{X}_R^{t+1}=\left(\rho\mathbf{I}_{|\mathbb{D}|}+\frac{\rho}{2}\mathbf{Y}_R\mathbf{Y}_R^T\right)^{-1}\left(\left(\frac{1}{4|\mathbb{D}|}+\frac{\tau}{2}\right)\mathbf{Y}_R+\rho\mathbf{Z}_R^t+\mathbf{\Lambda}_{1_R}^t+\frac{\rho}{2}\mathbf{Y}_R\mathbf{G}^t\right), \tag{33}$$

$$\mathbf{X}_S^{t+1}=\left(\rho\mathbf{I}_{|\mathbb{D}|}+\frac{\rho}{2}\mathbf{Y}_S\mathbf{Y}_S^T\right)^{-1}\left(\left(\frac{1}{4|\mathbb{D}|}+\frac{\tau}{2}\right)\mathbf{Y}_S+\rho\mathbf{Z}_S^t+\mathbf{\Lambda}_{1_S}^t+\frac{\rho}{2}\mathbf{Y}_S\mathbf{G}^t\right), \tag{34}$$

$$\mathbf{W}^{t+1}=\frac{1}{2}\mathbf{Z}_3^t+\frac{1}{2}\left(\mathbf{Z}_3^t\right)^H+\frac{1}{\rho}\left(\mathbf{\Lambda}_3^t-\frac{\tau}{2}\mathbf{I}_2\right), \tag{35}$$

$$\mathbf{u}^{t+1}=\frac{1}{\rho}\cdot\mathbf{\Psi}\cdot\mathrm{conj}\left(\mathscr{G}\left(\mathbf{\Lambda}_0^t\right)+\rho\mathscr{G}\left(\mathbf{Z}_0^t\right)-\frac{\tau}{2}|\mathbb{D}|\mathbf{e}_1\right), \tag{36}$$

where $\mathbf{a}=\mathscr{G}(\mathbf{A})$ is the mapping of a matrix to a vector, where the ***ith*** entry in $\mathbf{a}$ is the sum of all entries $\mathbf{A}_{j,\tilde{j}}$'s of $\mathbf{A}$, satisfying $j-\tilde{j}+1=\tilde{d}$ [29]. $\mathbf{\Psi}$ is a diagonal matrix with diagonal elements $\mathbf{\Psi}_{\tilde{d},\tilde{d}}=1/(|\mathbb{D}|-\tilde{d}+1),\tilde{d}=1,\cdots,|\mathbb{D}|$. The update of $\mathrm{Tr}(G)$ is expressed as

$$\mathrm{Tr}(\mathbf{G})^{t+1}=\left[\mathrm{Tr}\left[\left(1-\frac{\tau}{\rho}\right)\mathbf{I}_2-\mathbf{Y}_R^T\mathbf{X}_R^{t+1}\right]\right]_+. \tag{37}$$

Let

$$\mathbf{\Psi}^t=\begin{bmatrix}\mathbf{T}\left(\mathbf{u}^{t+1}\right) & \mathbf{X}_R^{t+1}+j\mathbf{X}_S^{t+1}\\ \left(\mathbf{X}_R^{t+1}+j\mathbf{X}_S^{t+1}\right)^H & \mathbf{W}^{t+1}\end{bmatrix}-\frac{1}{\rho}\mathbf{\Lambda}^t, \tag{38}$$

and $\mathbf{U}^t\ \mathrm{diag}\left(\{\sigma_{\tilde{d}}^t\}\right)(\mathbf{U}^t)^H$ is the eigenvalue decomposition of $\mathbf{\Psi}^t$. Then, the updated closed form expression of $\mathbf{Z}$ can be given as

$$\mathbf{Z}^{t+1}=\mathbf{U}^t\ \mathrm{diag}\left(\left\{\sigma_{\tilde{d}}^t\right\}\right)\left(\mathbf{U}^t\right)^H. \tag{39}$$

The reconstructed denoising measurements $\widehat{\mathbf{X}}$ can be obtained through the aforementioned closed form expressions. Next, two specific DOA estimation methods for the $\widehat{\mathbf{X}}$ will be introduced: SSRMUSIC algorithm and DP method.

4.3. One-Bit ADMM-SSRMUSIC Algorithm. One-Bit ADMM-SSRMUSIC first utilizes one-bit ADMM to reconstruct the measurements $\widehat{\mathbf{X}}$ and then estimates DOAs by SSRMUSIC. SSRMUSIC is the algorithm that obtains the covariance matrix with full rank by spatial smoothing [37] firstly and then finds the directions by Root-MUSIC [38]. In order to find directions by Root-MUSIC, $\widehat{\mathbf{X}}$ will be divided into $\tilde{L}$ subarrays, where $\tilde{L} = |\mathbb{D}| - D_{\max}$. The subarray can be expressed as $\widehat{\mathbf{X}}_{\tilde{l}}, \tilde{l} = 1, \cdots, \tilde{L}$. The full-rank covariance matrix can be obtained by the above operations.

$$\widehat{\mathbf{R}}_{\widehat{\mathbf{X}}_{\tilde{l}}} = \frac{1}{\tilde{L}} \sum_{\tilde{l}}^{\tilde{L}} E\left(\widehat{\mathbf{X}}_{\tilde{l}} \widehat{\mathbf{X}}_{\tilde{l}}^{H}\right). \tag{40}$$

Then, the DOAs can be estimated by Root-MUSIC based on Equation (40). The subspace algorithm is a very classical and well-known DOA estimation method, so we will not introduce the subspace algorithm in detail but focus on the DP method.

4.4. One-Bit ADMM-DP Algorithm. The first step of one-bit ADMM-DP is the same as one-bit ADMM-SSRMUSIC and then estimates DOAs by the DP method. Each norm has a corresponding dual norm. Compared with the original norms, dual norms have several useful properties and are widely used in many problems. The DP method transforms the optimal solution of the original problem to that of the dual problem. We can obtain the frequency support set and estimate the DOA [23, 29].

The Lagrangian corresponding to Equation (23) is

$$\begin{aligned} L(\mathbf{X}_R, \mathbf{X}_I, \operatorname{Tr}(\mathbf{G})) = {} & \tau \|\mathbf{X}\|_{\mathscr{A}} - \frac{1}{2|\mathbb{D}|} \operatorname{Tr}\left(\mathbf{Y}_R^T \mathbf{X}_R + \mathbf{Y}_S^T \mathbf{X}_S\right) \\ & + \operatorname{Tr}(\mathbf{G})\left[\operatorname{Tr}\left(\mathbf{Y}_R^T \mathbf{X}_R + \mathbf{Y}_S^T \mathbf{X}_S\right) - \operatorname{Tr}(\mathbf{I}_2)\right]. \end{aligned} \tag{41}$$

The dual function of Equation (41) is as follows:

$$\begin{aligned} g(\operatorname{Tr}(\mathbf{G})) &= \inf_{\mathbf{X}_R, \mathbf{X}_S} L(\mathbf{X}_R, \mathbf{X}_S, \operatorname{Tr}(\mathbf{G})) \\ &= -2\operatorname{Tr}(\mathbf{G}) + \inf_{\mathbf{X}_R, \mathbf{X}_S} \left[\tau\|\mathbf{X}\|_{\mathscr{A}} + \operatorname{Tr}(\mathbf{G})\operatorname{Tr}\left(\mathbf{Y}_R^T\mathbf{X}_R + \mathbf{Y}_S^T\mathbf{X}_S\right)\right. \\ &\quad \left. - \frac{1}{2|\mathbb{D}|}\operatorname{Tr}\left(\mathbf{Y}_R^T\mathbf{X}_R + \mathbf{Y}_S^T\mathbf{X}_S\right)\right] \\ &= -2\operatorname{Tr}(\mathbf{G}) + \inf_{\mathbf{X}_R, \mathbf{X}_S}\left[\tau\|\mathbf{X}\|_{\mathscr{A}} - \left(\frac{1}{2|\mathbb{D}|} - \operatorname{Tr}(\mathbf{G})\right)\operatorname{Tr}[\langle \mathbf{Y}, \mathbf{X}\rangle_R]\right] \\ &= -2\operatorname{Tr}(\mathbf{G}) + \inf_{\mathbf{X}_R, \mathbf{X}_S}\left[\tau\|\mathbf{X}\|_{\mathscr{A}} - \left\langle \left(\frac{1}{2|\mathbb{D}|} - \operatorname{Tr}(\mathbf{G})\right)\mathbf{Y}^*, \mathbf{X}\right\rangle_R\right] \\ &= -2\operatorname{Tr}(\mathbf{G}) + I_{\{\varpi : \|\varpi\|_A^* \le \tau\}}(\tilde{\mathbf{X}}), \end{aligned} \tag{42}$$

where $\tilde{\mathbf{X}} = (1/2|\mathbb{D}| - \operatorname{Tr}(\mathbf{G}))\mathbf{Y}^*$. $I_{\mathscr{A}}(\cdot)$ is an indicator function; the following formula can also be expressed as

$$I_{\{\varpi : \|\varpi\|_A^* \le \tau\}}(\tilde{\mathbf{X}}) = \begin{cases} 0, & \|\tilde{\mathbf{X}}\|_{\mathscr{A}}^* \le \tau, \\ -\infty, & \text{otherwise}. \end{cases} \tag{43}$$

From Equations (42) and (43), we have $\tau\|\mathbf{X}\|_{\mathscr{A}} - \langle \tilde{\mathbf{X}}, \mathbf{X}\rangle_R \le 0$,

$$\tau\|\mathbf{X}\|_{\mathscr{A}} \le \langle \tilde{\mathbf{X}}, \mathbf{X}\rangle_R. \tag{44}$$

The dual atomic norm is defined as

$$\|\tilde{\mathbf{X}}\|_{\mathscr{A}}^* = \sup_{\|\mathbf{X}\|_{\mathscr{A}} \le 1} \langle \tilde{\mathbf{X}}, \mathbf{X}\rangle_R = \sup_{\mathbf{A} \in \mathscr{A}} \langle \tilde{\mathbf{X}}, \mathbf{A}\rangle_R. \tag{45}$$

From the definition of dual atomic norm and $\|\tilde{\mathbf{X}}\|_{\mathscr{A}}^* \le \tau$, we can obtain

$$\langle \tilde{\mathbf{X}}, \mathbf{X}\rangle_R \le \|\tilde{\mathbf{X}}\|_{\mathscr{A}}^* \|\mathbf{X}\|_{\mathscr{A}} \le \tau\|\mathbf{X}\|_{\mathscr{A}}. \tag{46}$$

From Equations (44) and (46), we have $\langle \widehat{\tilde{\mathbf{X}}}, \widehat{\mathbf{X}}\rangle_R = \tau \|\widehat{\mathbf{X}}\|_{\mathscr{A}}$. It can be seen from Equations (17), (19), and (20), that $\widehat{\mathbf{A}}(f, \mathbf{b}) = \widehat{\mathbf{a}}_{\mathbb{D}}(f)\mathbf{b}^H$, $\widehat{\mathbf{X}} = \sum_{k=1}^{K} c_k \widehat{\mathbf{A}}(f_k, \mathbf{b}_k)$,
$\|\widehat{\mathbf{X}}\|_{\mathscr{A}} = \sum c_k$. Finally,

$$\left\langle \widehat{\tilde{\mathbf{X}}}, \widehat{\mathbf{a}}_{\mathbb{D}}(f)\right\rangle_R = \tau. \tag{47}$$

As a result, the signal frequencies can be recovered and DOAs can be estimated from Equation (47).

5. Simulation Results

Considering the nested array $\mathbb{S} = \{1, 2, 3, 4, 5, 6, 12, 18, 24, 30\}$, the difference array corresponding to $\mathbb{S}$ is $\mathbb{D} = \{0, \pm 1, \pm 2, \cdots, \pm 29\}$. $\varphi_k = [0, \pi/2]$ and $\psi_k = [-\pi, \pi]$ are obtained randomly. $p_k^2 = 1$ and $\boldsymbol{SNR} = 10 \log\left(\sum_{k=1}^{K} p_k^2 / 2k\sigma^2\right) = 10 \log\left(1/2\sigma^2\right)$. The performance of the DOA estimation is measured by the mean-square error (MSE) as

$$\text{MSE} = \frac{1}{RK} \sum_{r}^{R} \sum_{k}^{K} \left(\bar{\theta}\wedge_{r,k} - \bar{\theta}_k\right)^2, \tag{48}$$

where R means Monte Carlo runs, $R = 500$.

In order to show the advantages of the combination of the nested cross-dipole array and one-bit ADMM, the spatial spectrums are used to show the maximum number of sources that can be estimated. Figure 2 shows two spatial spectrums obtained by one-bit ADMM-SS-MUSIC and one-bit SS-MUSIC, respectively. One-bit ADMM-SS-MUSIC first reconstructs denoising measurements with one-bit ADMM and then estimates DOAs by SS-MUSIC, while one-bit SS-MUSIC estimates DOAs directly by SS-MUSIC [22]. The number of snapshots $N = 100$ and SNR $= 0$ dB. The number of sources $K = D_{\max} = 29$. The sources are uniformly distributed on $[-0.49, 0.49]$. Assuming that there are five CP signals, six UP sources, and eighteen PP signals, let the DOP of six PP signals are $\eta_k = 0.25$ and that of six PP signals are $\eta_k = 0.5$,; the rest of PP signals are $\eta_k = 0.75$. We can see that 29 sources are completely estimated by one-bit ADMM-SS-MUSIC. Obviously, $K = 29 > |\mathbb{S}| = 10$

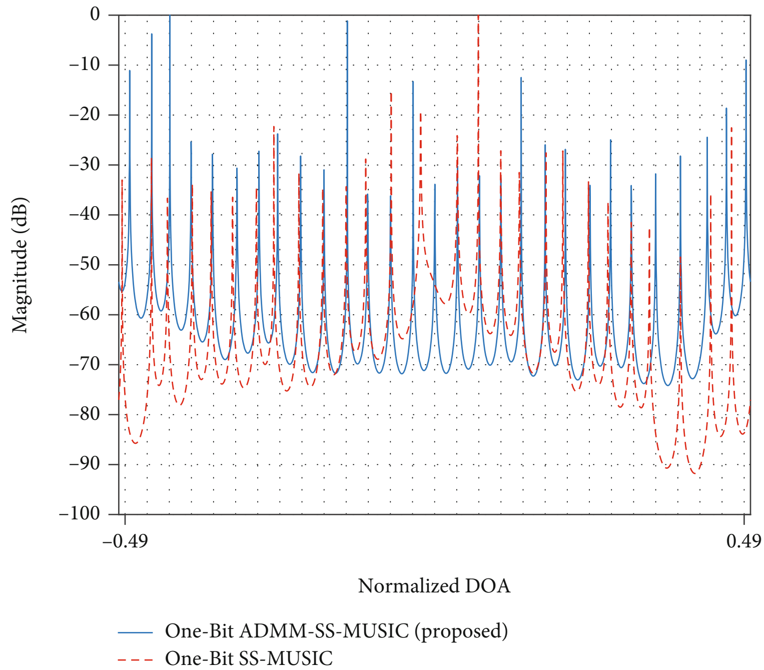

Figure 2: Spatial spectrum.

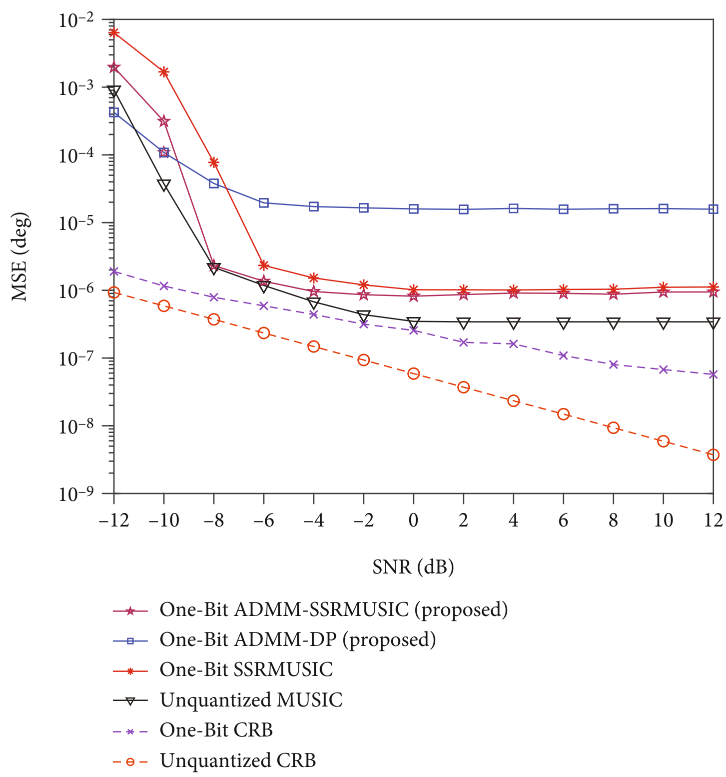

Figure 3: MSE versus the SNR.

. One-bit SS-MUSIC can only roughly estimate less than 29 sources, and the angle deviation is larger than one-bit ADMM-SS-MUSIC. It can infer that the algorithm will estimate more sources and improve the reliability if the signal is reconstructed by one-bit ADMM firstly.

Next, we consider the following DOA estimation algorithms:

(1) One-bit ADMM-SSRMUSIC: the gridless algorithm proposes in this paper

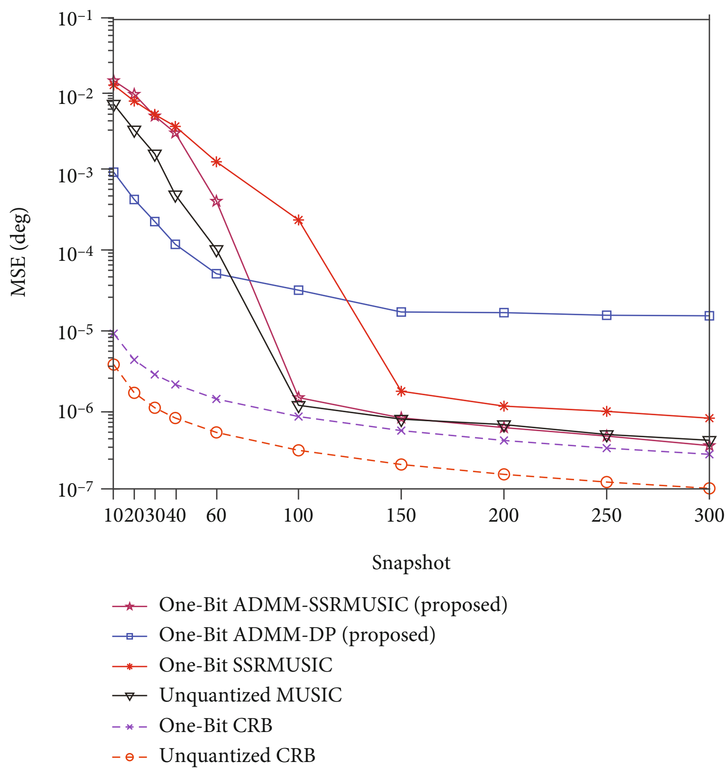

FIGURE 4: MSE versus the number of snapshots N.

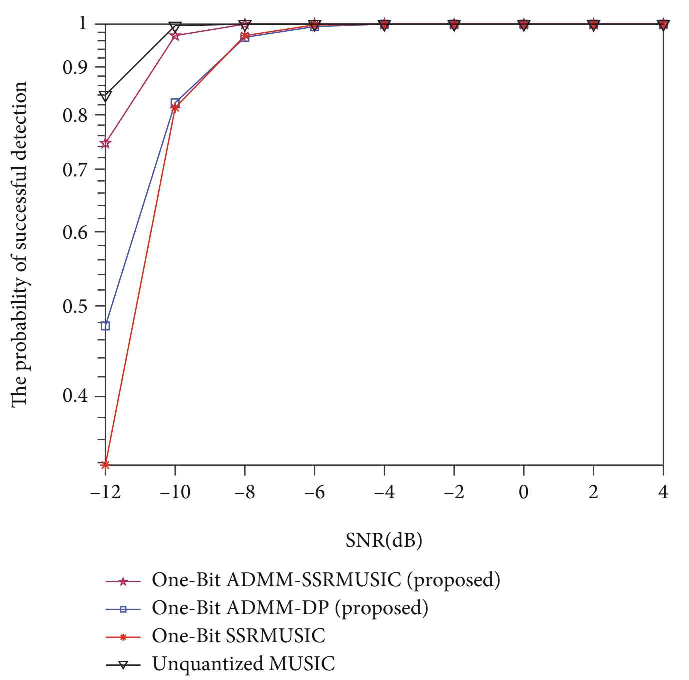

FIGURE 5: PSD versus the SNR.

(2) One-bit ADMM-DP: the gridless algorithm proposes in this paper

(3) One-bit SSRMUSIC: the method describes in [22], which finds directions directly by one-bit SS-Root-MUSIC

(4) Unquantized MUSIC: the method describes in [18], which is an unquantized method, and estimates DOAs by SS-MUSIC

Figure 3 illustrates the MSEs and Cramer-Rao bounds (CRBs) [22] versus the SNR with $N = 100$, $K = 5$, and $\overline{\theta}_k \in$

$\{-0.4,-0.2,0,0.2,0.4\}$. The sources are divided into one CP signal, one UP signal, and three PP signals with $\eta_k=\{0, 0.25, 0.5, 0.75, 1\}$. If there is no special explanation, $\overline{\theta}_k$ and η_k of the sources will not change in the next simulation. It can be seen from Figure 3 that one-bit ADMM-DP has higher estimation accuracy than one-bit ADMM-SSRMUSIC and one-bit SSRMUSIC at low SNR. The accuracy of one-bit ADMM-DP even exceeds the unquantized MUSIC when SNR is near -12 dB. When SNR is less than about 9 dB, one-bit ADMM-DP has better performance than one-bit ADMM-SSRMUSIC. The accuracy of one-bit ADMM-SSRMUSIC is much higher than that of one-bit SSRMUSIC at low SNR, and the accuracy gap between them gradually decreases with SNR increasing. Obviously, ADMM is very effective for improving the accuracy of DOA estimation, especially at low SNR.

Figure 4 illustrates the MSEs and CRBs versus the number of snapshots with SNR $=-6$ dB, $K=5$. In the range of $N=10$ to $N=60$, the estimation accuracy of one-bit ADMM-DP is higher than that of the other three algorithms. In addition, when the number of snapshots is less than about 80, one-bit ADMM-DP has better performance than one-bit ADMM-SSRMUSIC. It can be seen that the DP method is robust in the low snapshot. Besides, the accuracy of one-bit ADMM-SSRMUSIC and unquantized MUSIC is very close between $N=100$ and $N=300$. It reveals that the one-bit ADMM-SSRMUSIC and unquantized MUSIC have comparable performance in certain SNR and snapshot ranges. One-bit ADMM-SSRMUSIC and one-bit SSRMUSIC have almost the same recovery accuracy between $N=10$ and $N=40$, but the estimation accuracy of one-bit ADMM-SSRMUSIC is higher than that of one-bit SSRMUSIC with the increase of the number of snapshots. It can be recognized that the introduction of ADMM greatly improves performance.

Figure 5 shows the probability of a successful detection (PSD) versus the SNR with $N=100$, $K=5$. The PSD of the algorithms proposed in this paper (one-bit ADMM-SSRMUSIC and one-bit ADMM-DP) is higher than one-bit SSRMUSIC. In particular, one-bit ADMM-SSRMUSIC can achieve a 100% success rate at low SNR.

6. Conclusion

The one-bit ADMM on a nested cross-dipole array with the MMV model is used to estimate the DOAs of EM sources in this paper. Based on the properties of the cross-dipole array, one-bit ADMM is applied to the x-axis and y-axis dipole array and extended to the MMV model for solving the atomic norm minimization, the sign inconsistency will be solved and the basis mismatch will be avoided finally. The reconstructed signal denoising measurements will be obtained via one-bit ADMM. Finally, the SSRMUSIC algorithm and DP method are derived to estimate DOAs by the reconstructed denoising measurements. The simulation results show that the proposed algorithms are robust to DOA estimation of CP signals and PP signals, and ADMM is an effective method to improve the accuracy of DOA estimation. The one-bit ADMM-SSRMUSIC has a better performance than the one-bit SSRMUSIC in DOA estimation. Moreover, the accuracy of one-bit ADMM-DP is even surpassing that of unquantized MUSIC at low SNR and low snapshot.

Data Availability

No data were used to support this study.

Conflicts of Interest

The authors declare that there is no conflict of interest regarding the publication of this paper.

Acknowledgments

The study was supported by the Key Research and Development Program of Hainan Province (grant number 230 ZDYF2019011), the National Natural Science Foundation of China (grant numbers 61701144, 61861015 231, and 61961013), the Program of Hainan Association for Science and Technology Plans to Youth R&D 232 Innovation under grant number QCXM201706, the scientific research projects of University in Hainan Province 233 under grant number Hnky2018ZD-4, the Young Elite Scientists Sponsorship Program by CAST under grant number 234 2018QNRC001, the Collaborative Innovation Fund of Tianjin University and Hainan University under grant number 235 HDTDU201906, and the Scientific Research Setup Fund of Hainan University under grant number KYQD(ZR)1731 and National Natural Science Foundation of China (61701144, 61801076, and 61701533).

References

[1] J. Li and R. T. Compton, "Angle and polarization estimation using ESPRIT with a polarization sensitive array," *IEEE Transactions on Antennas and Propagation*, vol. 39, no. 9, pp. 1376–1383, 1991.

[2] J. Li and R. T. Compton, *Angle estimation using a polarization sensitive array*, vol. 1, Antennas and Propagation Society Symposium 1991 Digest, London, Ontario, Canada, 1991.

[3] J. Li, "On polarization estimation using a polarization sensitive array," in *IEEE Sixth SP Workshop on Statistical Signal and Array Processing*, pp. 465–468, Victoria, BC, Canada, 1992.

[4] J. He, M. O. Ahmad, and M. N. S. Swamy, "Near-field localization of partially polarized sources with a cross-dipole array," *IEEE Transactions on Aerospace and Electronic Systems*, vol. 49, no. 2, pp. 857–870, 2011.

[5] K. Wang, J. He, T. Shu, and Z. Liu, "Localization of mixed completely and partially polarized signals with crossed-dipole sensor arrays," *Sensors*, vol. 15, no. 12, pp. 31859–31868, 2015.

[6] C. L. Liu and P. P. Vaidyanathan, "One-bit sparse array DOA estimation," *2017 IEEE International Conference on Acoustics, Speech and Signal Processing (ICASSP)*, pp. , 20173126–3130, 2017.

[7] R. Schmidt, "Multiple emitter location and signal parameter estimation," *IEEE Transactions on Antennas and Propagation*, vol. 34, no. 3, pp. 276–280, 1986.

[8] R. Roy and T. Kailath, "ESPRIT-estimation of signal parameters via rotational invariance techniques," *IEEE Transactions on Acoustics, Speech, and Signal Processing*, vol. 37, no. 7, pp. 984–995, 1989.

[9] A. Moffet, "Minimum-redundancy linear arrays," *IEEE Transactions on Antennas and Propagation*, vol. 16, no. 2, pp. 172–175, 2003.

[10] P. Pal and P. P. Vaidyanathan, "Nested arrays: a novel approach to array processing with enhanced degrees of freedom," *IEEE Transactions on Signal Processing*, vol. 58, no. 8, pp. 4167–4181, 2010.

[11] P. P. Vaidyanathan and P. Pal, "Sparse sensing with co-prime samplers and arrays," *IEEE Transactions on Signal Processing*, vol. 59, no. 2, pp. 573–586, 2011.

[12] P. Pal and P. P. Vaidyanathan, "Coprime sampling and the music algorithm," in *2011 Digital Signal Processing and Signal Processing Education Meeting (DSP/SPE)}*, pp. 289–294, 2011.

[13] S. Qin, Y. D. Zhang, and M. G. Amin, "Generalized coprime array configurations for direction-of-arrival estimation," *IEEE Transactions on Signal Processing*, vol. 63, no. 6, pp. 1377–1390, 2015.

[14] A. Cui, T. Xu, and W. Yu, "An array interpolation based compressive sensing DOA method for sparse array," in *2019 3rd International Conference on Imaging, Signal Processing and Communication (ICISPC)*, pp. 24–27, 2019.

[15] Y.-k. Zhang, H.-y. Xu, R. Zong, B. Ba, and D.-m. Wang, "A novel high degree of freedom sparse array with displaced multistage cascade subarrays," *Digital Signal Processing*, vol. 90, pp. 36–45, 2019.

[16] S. Li and X. P. Zhang, "A new approach to construct virtual array with increased degrees of freedom for moving sparse arrays," *IEEE Signal Processing Letters*, vol. 27, pp. 805–809, 2020.

[17] J. Shi, F. Wen, and T. Liu, *Nested MIMO Radar: Coarrays, Tensor Modeling and Angle Estimation*, IEEE Transactions on Aerospace and Electronic Systems, 2020.

[18] J. He, Z. Zhang, T. Shu, and W. Yu, "Direction finding of multiple partially polarized signals with a nested cross-diople array," *IEEE Antennas and Wireless Propagation Letters*, vol. 16, pp. 1679–1682, 2017.

[19] L. Pan, S. Xiao, and B. Li, "Continuous-time signal recovery from 1-bit multiple measurement vectors," *AEU-International Journal of Electronics and Communications*, vol. 76, pp. 132–136, 2017.

[20] T. Chen, M. Guo, and X. Huang, "Direction finding using compressive one-bit measurements," *IEEE Access*, vol. 6, pp. 41201–41211, 2018.

[21] Y. Gao, D. Hu, Y. Chen, and Y. Ma, "Gridless 1-b DOA estimation exploiting SVM approach," *IEEE Communications Letters*, vol. 21, no. 10, pp. 2210–2213, 2017.

[22] Z. Cheng, S. Chen, and Q. Shen, "Direction finding of electromagnetic sources on a sparse cross-dipole array using one-bit measurements," *IEEE Access*, vol. 8, pp. 83131–83143, 2020.

[23] Z. Wei, W. Wang, and F. Dong, "Gridless one-bit direction-of-arrival estimation via atomic norm denoising," *IEEE Communications Letters*, vol. 24, no. 10, pp. 2177–2181, 2020.

[24] G. Tang, B. N. Bhaskar, and P. Shah, "Compressed sensing off the grid," *IEEE Transactions on Information Theory*, vol. 59, no. 11, pp. 7465–7490, 2013.

[25] L. Wan, X. Kong, and F. Xia, "Joint range-Doppler-angle estimation for intelligent tracking of moving aerial targets," *IEEE Internet of Things Journal*, vol. 5, no. 3, pp. 1625–1636, 2018.

[26] F. Wen and J. Shi, "Fast direction finding for bistatic EMVS-MIMO radar without pairing," *Signal Process*, vol. 173, p. 107512, 2020.

[27] X. Wang, M. Huang, and L. Wan, *Joint 2D-DOD and 2D-DOA Estimation for Coprime EMVS-MIMO Radar*, Circuits, Systems, and Signal Processing, accept, 2020.

[28] S. Boyd, N. Parikh, and E. Chu, "Distributed optimization and statistical learning via the alternating direction method of multipliers," *Foundations and Trends in Machine Learning*, vol. 3, no. 1, pp. 1–122, 2010.

[29] Y. Li and Y. Chi, "Off-the-grid line spectrum denoising and estimation with multiple measurement vectors," *IEEE Transactions on Signal Processing*, vol. 64, no. 5, pp. 1257–1269, 2016.

[30] Wong, L. Li, and Zoltowski, "Root-MUSIC-based direction-finding and polarization estimation using diversely polarized possibly collocated antennas," *IEEE Antennas and Wireless Propagation Letters*, vol. 3, pp. 129–132, 2004.

[31] Y. Merah, S. Miron, and D. Brie, "A generalized acquisition scheme for vector cross-product direction finding with spatially spread vector-sensor components," *2013 IEEE International Conference on Acoustics, Speech and Signal Processing*, 2013, pp. 3977–3980, Vancouver, BC, 2013.

[32] D. Rahamim, J. Tabrikian, and R. Shavit, "Source localization using vector sensor array in a multipath environment," *IEEE Transactions on Signal Processing*, vol. 52, no. 11, pp. 3096–3103, 2004.

[33] C. Liu and P. P. Vaidyanathan, "New Cramer-Rao bounds for coprime and other sparse arrays," *2016 IEEE Sensor Array and Multichannel Signal Processing Workshop (SAM)*, pp. , 20161–5, 2016.

[34] V. Chandrasekaran, B. Recht, P. A. Parrilo, and A. S. Willsky, "The convex geometry of linear inverse problems," *Foundations of Computational Mathematics*, vol. 12, no. 6, pp. 805–849, 2012.

[35] R. T. Rockafellar, *Convex Analysis*, Princeton University Pre, 1970.

[36] F. F. BONSALL, "A general atomic decomposition theorem and Banach's closed range theorem," *Quarterly Journal of Mathematics*, vol. 42, no. 1, pp. 9–14, 1991.

[37] M. L. McCloud and L. L. Scharf, "A new subspace identification algorithm for high-resolution DOA estimation," *IEEE Transactions on Antennas and Propagation*, vol. 50, no. 10, pp. 1382–1390, 2002.

[38] B. D. Rao and K. V. S. Hari, "Performance analysis of root-music," *IEEE Transactions on Acoustics, Speech, and Signal Processing*, vol. 37, no. 12, pp. 1939–1949, 1989.